Published in final edited form as:

Inorg Chem. 2019 November 04; 58(21): 14532–14541. doi:10.1021/acs.inorgchem.9b02122.

Elusive Valence Transition in Mixed-Valence Sesquioxide Cs_4O_6

Ross H. Colman[†], **H. Esma Okur**[‡], **Winfried Kockelmann**[§], **Craig M. Brown**[⊥], **Annette Sans**[‖], **Claudia Felser**[¶], **Martin Jansen**[‖], **Kosmas Prassides**[*,∇,#]

[†]Department of Condensed Matter Physics, Faculty of Mathematics and Physics, Charles University, Prague 121 16, Czech Republic

[‡]Department of Chemistry, Faculty of Engineering and Natural Sciences, Bursa Technical University, Bursa TR-16310, Turkey

[§]ISIS Facility, Science and Technology Facilities Council, Rutherford Appleton Laboratory, Harwell OX11 0QX, United Kingdom

[⊥]Center for Neutron Research, National Institute of Standards and Technology (NIST), Gaithersburg, Maryland 20899, United States

[‖]Max Planck Institute for Solid State Research, Heisenbergstrasse 1, Stuttgart 70569, Germany

[¶]Max Planck Institute for Chemical Physics of Solids, Nöthnitzer Straße 40, Dresden 01187, Germany

[∇]Department of Materials Science, Graduate School of Engineering, Osaka Prefecture University, Osaka 599-8531, Japan

[#]Advanced Institute for Materials Research (WPI-AIMR), Tohoku University, Sendai 980-8577, Japan

Abstract

Cs_4O_6 is a mixed-valence molecular oxide with a cubic structure, comprising valency-delocalized $O_2^{4/3-}$ units and with properties highly sensitive to cooling protocols. Here we use neutron powder diffraction to authenticate that, while upon deep quenching the cubic phase is kinetically arrested down to cryogenic temperatures, ultraslow cooling results in an incomplete structural transition to a contracted tetragonal phase. Two dioxygen anions in a 1:2 ratio are identified, providing evidence that the transition is accompanied by charge and orbital order and stabilizes a Robin–Day Class II mixed-valence state, comprising O_2^{2-} and O_2^{-} anions. The phenomenology of the phase change is consistent with that of a martensitic transition. The response of the low-temperature phase assemblage to heating is complex, involving a series of successive interconversions between the coexisting phases. Notably, a broad interconversion plateau is present near 260 K, signifying reentrant kinetic arrest of the tetragonal phase upon heating because of the combined effects of

[*]**Corresponding Author** k.prassides@mtr.osakafu-u.ac.jp (K.P.).

Supporting Information

The Supporting Information is available free of charge on the ACS Publications website at DOI: 10.1021/acs.inorgchem.9b02122. Additional details of the NPD structural refinements, including Rietveld refinement plots, tables of refined parameters, and further structural information (PDF)

The authors declare no competing financial interest.

increased steric hindrance for molecular rotation and melting of charge and orbital order. The geometrically frustrated pyrochlore lattice adopted by the paramagnetic $S = ½$ O_2^- units provides an intimate link between the crystal and magnetic properties of charge-ordered Cs_4O_6, naturally accounting for the absence of magnetic order.

Graphical Abstract

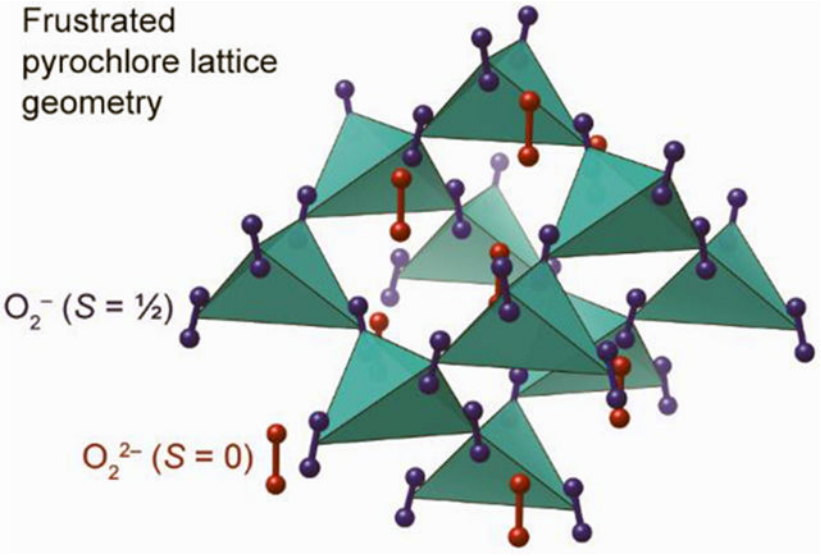

INTRODUCTION

The electronic properties of materials arising from d and f shells have drawn the bulk of research attention in condensed matter science, but although unconventional p-electron-based electronic, magnetic, and conducting properties are somewhat rare, they represent a fascinating topic (e.g., unconventional high-T_c superconductivity proximate to antiferromagnetic order in strongly correlated molecular fullerides[1] and quantum spin liquid states in Mott insulating ionic salts of polyaromatic hydrocarbons[2]) that presents the added challenge of molecular structural and electronic complexity. In particular, molecular oxygen forms a number of saltlike solids when combined with alkali metals. Among the alkali oxides, the molecular sesquioxides A_4O_6 (A = alkali metal) are of special interest. In contrast to other related compounds such as A_2O_2 and AO_2, which are white, yellow, or orange, the sesquioxides Rb_4O_6 and Cs_4O_6 are black. Their formula can be represented as $(A^+)_4(O_2^-)_2(O_2^{2-})$, comprising three molecular anions, one closed-shell nonmagnetic peroxide anion, O_2^{2-}, and two open-shell magnetic ($S = ½$) superoxide anions, O_2^-.[3,4] The alkali-metal sesquioxides are therefore rare examples of binary ionic compounds with dioxygen in two different charge states–mixed-valence molecular oxides.[5,6]

Powder X-ray diffraction work originally found that Rb_4O_6 and Cs_4O_6 adopt the cubic anti-Th_3P_4 structure (or Pu_2C_3 structure, space group $I\bar{4}3d$)[7] in which the two different molecular oxide anions remain indistinguishable, implying the presence of a single average-valency (delocalized) $[O—O]^{4/3-}$ unit. This finding was subsequently confirmed by single-crystal X-

ray diffraction on Rb_4O_6.[3] However, a very fundamental structural and electronic issue soon emerged. Specifically, when the structure of the lighter analogue Rb_4O_6 was studied by neutron powder diffraction (NPD) down to 5 K, no deviation from cubic symmetry was observed. On the other hand, both Raman and neutron inelastic spectroscopic studies provided unambiguous evidence for the presence of anion mixed valency through the observation of distinct vibrational modes at different frequencies associated with the two differently charged dioxygen units, O_2^{2-} and O_2^{-}.[4,8] So, although Rb_4O_6 and Cs_4O_6 appeared to be crystallographically single-valent, spectroscopy provided unambiguous evidence for two localized valence states of dioxygen.

The controversial structural results also reflected the existence of conflicting interpretations of the electronic properties of the sesquioxides in the absence of direct experimental structural determination. Electronic structure calculations using the local spin-density approximation proposed half-metallic ferromagnetism in Rb_4O_6.[9] However, experimental investigation of the temperature-dependent magnetization of Rb_4O_6 found no direct indication of ferromagnetic behavior. Instead, the results were consistent with the behavior of a magnetically frustrated insulator that exhibits a spin-glass-like response in a magnetic field. This was explained by random localization of the four additional electrons on the three charged dioxygen molecules in each formula unit on a cubic lattice, i.e., a valence localized but a charge-disordered state.[10] Theoretical studies also confirmed the insulating ground state and magnetic frustration due to the existence of nonmagnetic peroxide and magnetic superoxide anions that assemble in a frustrated antiferromagnetic configuration in cubic Rb_4O_6.[11] The existence of magnetic frustration was also proposed for cubic-structured Cs_4O_6.[8]

Significant advances in gradually resolving the conflicting structural and electronic properties have been made in more recent work. In particular, the results of NMR and electron paramagnetic resonance (EPR) spectroscopic measurements of Cs_4O_6 were found to be sensitively affected by different cooling protocols of the sample, suggesting nonequilibrium behavior.[12] The data were interpreted in terms of a transition to a low-symmetry phase at low temperatures in which the degeneracy of the antibonding π^* molecular orbitals is removed and orbital ordering occurs. This then affects the magnetic properties via modulation of the superexchange interactions through the Cs^+ bridges. Pronounced anomalies in the temperature dependence of the magnetic susceptibility of Cs_4O_6 were evident between 200 and 250 K and at 320 K.[12] At the same time, single-crystal X-ray diffraction of the lighter-element analogue, Rb_4O_6, established the symmetry of its low-temperature phase at 100 K as tetragonal and proposed the $I\bar{4}$ space group as appropriate.[13] Finally, detailed structural and spectroscopic work on Cs_4O_6 confirmed the phase change from cubic (charge-disordered) to tetragonal (charge-ordered) reminiscent of a Verwey-like charge-ordering transition, which is accompanied by a drop in the electronic conductivity.[14]

Here we report the results of a comprehensive series of temperature-dependent high-resolution NPD measurements of the crystal structure of Cs_4O_6 under a variety of thermal protocols designed to disentangle the true nature of its elusive low-temperature phase by bypassing kinetic arrest of the high-temperature phase. Our work unveils and maps out in

detail a complex cubic (charge-disordered)–tetragonal (charge-ordered) stability phase space together with an intimate link between the lattice geometry—a frustrated pyrochlore lattice arrangement—of the magnetic (S = ½) superoxide anions, O_2^-, in the contracted tetragonal charge-ordered phase and the absence of long-range magnetic ordering. The diffusionless character of the first-order transformation, which is driven by the concerted rotation of $^2/_3$ of the dioxygen molecular anions, is consistent with its classification as a martensitic transition.[15]

EXPERIMENTAL SECTION

The Cs_4O_6 sample used in the present study was prepared by a direct solid-state reaction, as described before.[12] Because Cs_4O_6 is extremely air- and moisture-sensitive, all subsequent sample manipulations were performed in inert-gas-filled gloveboxes (H_2O and O_2 < 0.1 ppm).

NPD experiments were first undertaken with the high-resolution diffractometer BT1 at the Center for Neutron Research, NIST, Gaithersburg, Maryland. Rapid cooling of the sample was achieved by “deep quenching” from 320 K into liquid nitrogen under an inert atmosphere, followed by transfer to the cryostat for further cooling. Diffraction measurements were performed upon warming. The temperature of the sample was then raised to 320 K before slow cooling at 12 K h^{-1}. Data were again collected upon warming. See the Supporting Information (SI) for further experimental details. Data analysis was performed with the GSAS suite of powder diffraction software.[16]

Time-of-flight NPD (tof-NPD) experiments were next undertaken with the multidetector, high-resolution General Materials (GEM) diffractometer at the ISIS Facility, Rutherford Appleton Laboratory, Harwell, U.K. The sample was again first heated to 320 K, and all subsequent cooling and heating treatments of the sample were performed in a manner analogous to those first employed at NIST. Following “deep quenching”, diffraction data were collected continuously upon warming. The sample was then held at 320 K before “ultraslow cooling” from 320 to 50 K at a rate of 1.68 K h^{-1} and then cooled more rapidly to 1.8 K. Diffraction data were again collected continuously upon warming. Following equilibration at 320 K, data were then collected continuously while cooling at a rate of 12 K h^{-1} to 140 K (“slow cooling” procedure). Extended experimental details can be found in the SI.

RESULTS

Exploratory NPD under Different Thermal Protocols.

Preliminary high-resolution NPD data, collected with the BT1 diffractometer at 300 K, confirmed adoption of the previously reported cubic Pu_2C_3 structure (space group $I\bar{4}3d$).[17] A stark difference in the temperature evolution of the diffraction data is observed, however, upon warming after either the previously described “deep-quenching” or “slow-cooling” protocols were employed. After “deep-quenching” at 10 K, all diffraction peaks can be indexed with the cubic $I\bar{4}3d$ space group, with no sign of additional reflections that could have indicated a temperature-induced structural phase transition (Figure 1a).

Rietveld analysis of the data (selected patterns and resulting structural parameters available as SI, Figure S1, and Table S1) shows no significant structural changes besides the expected lattice contraction upon cooling. Upon warming from this “deep-quenched” state to 172 K, additional reflections appear that can no longer be indexed by the cubic structure but instead fit the reported tetragonal structure with space group $I\bar{4}2d$.[13] The existence of both tetragonal and cubic reflections indicates phase coexistence, suggesting that the structural transition is first order. Upon further warming to 250 K, the relative intensities of the cubic peaks increase at the expense of the tetragonal peaks, and by 300 K, the tetragonal phase has been almost completely converted to cubic.

After the “slow-cooling” procedure, the data collected at 10 K show the coexistence of Bragg reflections originating from both the cubic and tetragonal structures, implying that a fraction of the cubic phase is still frozen in, despite the extremely slow cooling thermal treatment (Figures 1b and S2 and Table S2). Upon warming to 130 K from the “slow-cooled” state, no significant change in the refined phase fractions is seen. However, further warming to 170 K results in a significant increase in the relative intensity of the tetragonal phase peaks, a trend that is reversed upon further heating to 250 K. As the temperature is increased to 300 K, the cubic peaks continue to grow in intensity at the cost of those of the tetragonal phase, and at 320 K, there is no longer evidence of the tetragonal phase (Figure S3 and Table S1). These exploratory measurements have unveiled a complex thermal history dependence of the structural properties of the material that merits further detailed investigation.

Cubic Cs_4O_6 at High Temperature.

The results of the detailed Rietveld analysis of the high-statistics tof-NPD data (Figure 2a) collected at 320 K are in agreement with both earlier structural determinations[3,4,7] and the conclusions drawn by the angular-dispersive diffraction experiments at NIST (vide supra). They readily reveal the adoption of a cubic (C) unit cell (a_C = 9.86744(8) Å; space group $I\bar{4}3d$), with symmetry-equivalent oxygen atoms residing in the 24d position. The single oxygen crystallographic position, seen by diffraction, which probes the time- and space-averaged structure, is consistent with the presence of indistinguishable molecular anions, i.e., single average-valency $(O{-}O)^{4/3-}$ dimeric units (Figure 3a) at high temperature. Some additional peaks are also evident in the diffraction data and these can be accounted for by the presence of a minority cubic CsO_2 phase[18] [a_{CsO_2} = 6.5864(7) Å; space group $Fm\bar{3}m$; 4.9(2)% fraction; Table 1]. An expanded discussion of the refined structural features can be found in the SI.

“Deeply Quenched” Cs_4O_6 and Its Structural Response to Heating.

Inspection of the tof-NPD profile of the sample at 10 K following the “deep-quenching” thermal procedure (Figure 2b) confirmed the survival of the strictly cubic (C) unit cell (a_C = 9.75760(5) Å; space group $I\bar{4}3d$; Figure 3a) adopted at 320 K. We note that the CsO_2 impurity phase is no longer evident; because of a symmetry-lowering transformation from cubic to tetragonal, the associated peak splitting spreads out the intensity such that it is smeared out into the background. Rietveld analysis of the diffraction data confirms that there

is only one symmetry-distinct dioxygen species consistent with the presence of valency-delocalized $(O—O)^{4/3-}$ dimeric units down to 10 K.

Using tof-NPD data collected after the sample is cooled from 10 to 1.8 K, we find evidence neither for the emergence of magnetic Bragg peaks nor for a change in diffuse scattering, supporting the absence of long- or short-range magnetic order in quenched cubic Cs_4O_6 down to 1.8 K (Figure S5).

The response of the tof-NPD patterns of "deeply quenched" cubic Cs_4O_6 to slow heating (Figures 4a and S6) mirrors the behavior unveiled by the exploratory NPD measurements on BT1 and confirms that the cubic structure is initially robust up to 164 K. The Rietveld refinements in this temperature range proceed routinely, revealing only a monotonic increase in the cubic lattice constant and unit cell volume with increasing T (Figure 5). However, as the sample is heated further above 164 K, a new set of diffraction peaks whose intensities grow at the expense of that of the Bragg reflections of the "deeply quenched" cubic phase and saturate rapidly at ~195 K emerge, signifying the onset of structural transformation. Further growth in the intensities of the new peaks is arrested until about 220 K. Accordingly, the NPD profiles in this temperature range were refined using a model of coexisting tetragonal (T) and cubic (C) phases. The tetragonal unit cell [space group $I\bar{4}2d$; lattice metrics a_T = 9.2875(6) Å, c_T = 10.8571(15) Å, V_T = 936.5(2) Å^3; phase fraction = 75.2(1)% at 200 K; Figure 6] is shown in Figure 3b. Notably, there is a pronounced contraction of the ab basal plane, together with an expansion of the c axis compared to the lattice dimensions of the cubic cell at the same temperature [a_C = 9.8144(4) Å and V_C = 945.4(1) Å at 200 K], resulting in an overall contraction of the unit cell volume by 0.94(2)% (Figure 5). The severe renormalization of the lattice metrics can be easily understood by referring to the differences in the orientation of the dioxygen units between the two structures (Figure 3). While in the cubic unit cell, all dimers are aligned parallel to the three crystallographic axes, and in the tetragonal unit cell, $\frac{2}{3}$ of the dioxygen units flip by 73.8(2)° from their parallel orientation to the basal plane to point at an angle of 16.2(2)° toward the c axis. The remaining $\frac{1}{3}$ of the dimer units retain their strictly parallel orientation to the c axis.

These pronounced structural changes accompanying the C → T phase transition are a direct consequence of the occupation of two symmetry-inequivalent crystallographic sites, O(1) (8c) and O(2)(16e) by the oxygen atoms. This leads to two types of clearly identifiable dioxygen anions at a relative ratio of 1:2 and with two sets of distinct bond lengths [1.49(2) and 1.29(2) Å, respectively, at 200 K], implying that the structural transition is accompanied by the charge-ordering transformation, $3(O—O)^{4/3-} \rightarrow (O—O)^{2-} + 2(O—O)^{-}$, and the emergence of anion mixed valency. The molecular formula of T-structured Cs_4O_6 can thus be represented as $(Cs^+)_4(O_2^{2-})(O_2^-)_2$. Heating past 220 K initially leads to a reduction in the intensity of the Bragg reflections of the tetragonal phase with concomitant recovery of the intensity of the cubic phase reflections (Figures 4a and S6). However, above 266 K, the phase fractions of the two coexisting phases remain invariant at 57(1)% (T phase) and 42(1)% (C phase) until about 296 K, when the T → C transformation rapidly begins to proceed toward completion. However, the sluggish nature of the transition requires extensive thermal equilibration of the sample for a period of 2 h at 320 K (the highest temperature of

the present experiments) before complete conversion to cubic-structured Cs_4O_6 is achieved (Figure 6).

"Ultraslow-Cooled" Cs_4O_6 and Its Structural Response to Heating.

Simple inspection of the measured profile after ultraslow cooling (Figure 2c) shows a sharp contrast with that obtained following the "deep-quenching" protocol (Figure 2b). The pattern can be now indexed with two coexisting tetragonal and cubic cells. The Rietveld refinements proceeded smoothly (Figure 2c and Table 1), leading to results comparable to those obtained by analysis of the data sets collected at higher temperatures upon heating following the "deep quenching" procedure; the cell metrics of the majority [phase fraction 76.51(7)%] tetragonal phase are a_T = 9.1586(2) Å, c_T = 10.8653(5) Å, and V_T = 911.38(5) Å^3, while those of the minority cubic phase [phase fraction 23.5(2)%] are a_C = 9.7381(2) Å and V_C = 923.48(5) Å^3. The size of the latter is larger by 1.310(7)% at this temperature.

The two distinct dioxygen units in the charge-ordered phase refine as 1.528(6) Å for the O(1)—O(1) dimers, which are strictly aligned parallel to the *c* axis and 1.345(4) Å for the O(2)—O(2) dimers, which are inclined at an angle of 16.2(2)° to the *c* axis (Table 1). These values compare well with those reported before for tetragonal Cs_4O_6 (1.53 and 1.31 Å, respectively)[14] and are in excellent agreement with literature values for the O_2^{2-} [1.541(6) Å][20] and O_2^- [1.34(3) Å][21] dimeric units, respectively, unambiguously establishing the T-structured phase as valence-localized and charge-ordered $(Cs^+)_4(O_2^{2-})(O_2^-)_2$.

In a fashion similar to that in the case of cubic Cs_4O_6, tof-NPD measurements also support the absence of long- or short-range magnetic order in charge-ordered T-structured Cs_4O_6 down to 1.8 K (Figure S5).

The behavior of the Cs_4O_6 T- and C-phase assemblages upon slow heating (Figures 4b and S6) is essentially identical with that of the "deeply quenched" cubic Cs_4O_6. It remains unchanged until the temperature is raised to 164 K, whereupon, upon further heating, the tetragonal phase fraction begins to grow, quickly saturating to 85.6(1)% at 190 K and remaining unchanged to 212 K (Figure 6). Further heating leads to a sharp diminution (growth) of the tetragonal (cubic) phase fraction until a temperature of 266 K is reached when the phase fractions of the two coexisting phases remain invariant at 38(1)% (T phase) and 61(1)% (C phase) until about 296 K, when the T → C transformation is rapidly reinitiated, going to completion at 320 K after a 2 h equilibration.

The response of the tetragonal lattice constants *a* and *c* to the temperature is considerably anisotropic (Figure 5). We find that the basal plane dimensions expand normally upon heating at a rate of $\mathrm{d}\ln a_T/\mathrm{d}T \sim 90$ ppm K^{-1}, significantly higher than that of the cubic lattice constant ($\mathrm{d}\ln a_C/\mathrm{d}T \sim 50$ ppm K^{-1}). However, the expanded tetragonal c_T axis varies little over the whole temperature range, displaying an anomalous weak negative thermal expansion behavior ($\mathrm{d}\ln c_T/\mathrm{d}T \sim -20$ ppm K^{-1}). The anisotropic response of the unit cell reflects the fact that all molecular strongly bonded dioxygen units either are aligned parallel to or are inclined toward the *c* axis. This geometrical alignment confers the structure considerable stiffness along the *c* axis, while at the same time permitting the usual positive thermal expansion behavior of the basal plane. The anomalous behavior in the lattice metrics

above 250 K coincides with the onset of the plateau in the variation of the phase fractions of the coexisting C and T phases (Figure 6) vide infra.

Structural Response of Cubic Cs_4O_6 to "Slow Cooling".

No change is observed until the temperature reaches 198 K, whereupon, upon further cooling, the intensities of the Bragg reflections of the cubic phase begin to decrease rapidly, while, at the same time, a new set of reflections begins to grow (Figure 4c). The transformation to the contracted tetragonal phase does not go to completion and saturates within ~50 K to a phase fraction value of 53.6(1)% at 147 K (Figure 6), significantly smaller than that [76.6(1)%] achieved at the same temperature when the sample was cooled at a much slower rate (1.68 K h^{-1}). No further changes take place down to 140 K, the lowest temperature reached in these measurements. The C → T transformation is therefore strongly hysteretic and severely dependent on the cooling and heating thermal protocols employed in the experiments, implying nonequilibrium behavior.

DISCUSSION

The Cs_4O_6 system is complex, with a fine interplay of the charge, orbital, and rotational degrees of freedom. At high temperature, the high-symmetry cubic structure that describes the material infers either dynamic delocalization of the charge or static disorder because all dioxygen units are symmetry-equivalent. The time- and space-averaged structure probed by diffraction data is sensitive to valence ordering, which would cause symmetry breaking, or dynamics much slower than the neutron interaction time (~10^{-12}–10^{-13} s), which would give rise to a superposition of the two valence states, neither of which we observe. Previous complementary Raman, ^{17}O NMR, X-band EPR, and impedance spectroscopy studies have indicated dynamic charge hopping in the range 10^{-10}–10^{-13} s.[12] Upon cooling below ~200 K, these studies inferred the occurrence of charge localization, as evidenced, for instance, by transformation of the NMR line shapes from Lorentzian to Gaussian.[12] If cooling is allowed to occur slowly, charge localization is accompanied by charge ordering that induces a structural phase transition. Similar out-of-equilibrium kinetic arrest phenomena upon charge ordering have been previously studied in several rare-earth manganites.[22-24] In the valence-localized and charge-ordered tetragonal phase, the reduced symmetry allows two distinct O—O sites in a 1:2 ratio with significantly different bond lengths that confirm the presence of superoxide and peroxide groups. The material can therefore be described by the formula $(Cs^+)_4(O_2^-)_2(O_2^{2-})$ and classified as a Robin–Day Class II mixed-valence system. The O_2^- groups, containing an unpaired electron, are responsible for the magnetic response of this material, and careful consideration of its local environment is important when interpreting its magnetic properties. In the high-symmetry charge-disordered structure, all (symmetry-equivalent) O_2 groups align parallel with the crystallographic axes. The molecules are centered on a 12a virtual Wyckoff position, with −4.. site symmetry.[13] In such a symmetric environment, the unpaired electron resides in degenerate π^*_x and π^*_y molecular orbitals. However, in the low-temperature tetragonal structure, tilting of the O_2^- molecular units away from the crystallographic axis implies the occurrence of a Jahn–Teller distortion and selection of a single π^* orbital, i.e., orbital ordering.

It was previously suggested that the ~17° tilt of the O_2^- units away from the *c* axis reduces orbital overlap with neighboring Cs^+ ions and subsequently suppresses superexchange interactions, thereby preventing a transition to a magnetically ordered ground state.[14] However, close inspection of the local environment around the O_2^- units in the tetragonal phase shows that the tilting brings the molecular bonding axis into alignment with one specific pair of Cs^+ ions of the encapsulating polyhedron (Figures 7b and 8a), with an almost temperature-independent dihedral angle of <4° (Figure S7). It is not immediately clear whether this alignment might signify an increased electronic interaction between the O_2^- unit and one pair of Cs^+ ions or whether it is purely a result of steric effects. If the former is the case, it is important to note that no Cs^+ ion is aligned in this way with two O_2^- units. If magnetic exchange is mediated by these *aligned* Cs^+ ions, it will be through (O_2^-)–Cs^+–Cs^+–(O_2^-) supersuperexchange, consistent with the lack of magnetic order.

On the other hand, if magnetic exchange is not specifically mediated by these *aligned* Cs^+ ions, then (O_2^-)–Cs^+–(O_2^-) superexchange pathways exist and an alternative explanation for the lack of a magnetically ordered ground state is derived from the O_2^- lattice geometry. The O_2^- units of the tetragonal structure create a lattice of vertex-sharing tetrahedra, a distorted pyrochlore lattice (Figure 7c). The pyrochlore lattice is a canonical example of a magnetically frustrated lattice,[25] known to hinder the selection of a unique ground state, particularly in $S = ½$ quantum spin systems.[26]

A striking feature in the temperature dependence of the tetragonal lattice parameters is an anomalous expansion (contraction) of the *c* (*a*) axis upon heating above ~266 K, which results in a sudden increase in the *c*/*a* ratio. This anomaly is concomitant with an anomalous arrest of conversion of the tetragonal phase to the cubic phase upon warming above 260 K. In addition, the resulting phase transformation plateau between 260 and 300 K is observed during both experimentally employed heating protocols with no change in the experimental heating rate, confirming the intrinsic nature of the effect.

Despite this, we note that the system is not at equilibrium in this temperature range. The tetragonal phase is not the thermodynamic ground state but is observed because of the slow kinetics of its transformation to the cubic structure. While all transitions are reproducible, the nonequilibrium behavior is further highlighted by considering the difference in the phase fractions observed after various heating and cooling protocols are employed. Moreover, the plateau also explains the previously reported time independence of impedance measurements at 273 K.[14] Those measurements were used to conclude that the tetragonal structure is stable at all temperatures below the 310 K transformation. However, our results imply that the impedance measurement at 273 K accidentally lies within the plateau temperature range and in reality, and the transformation should have already been partially complete during the measurements at this temperature.

In order to explain the occurrence of the plateau, we examine in detail the temperature dependence of the refined structural parameters, and, in particular, we consider again the changes in the interaction between the O_2^- unit and its aligned pair of Cs^+ ions. During warming from 2 to 266 K, the distance between the center of the O_2^- anion and the midpoint of the separation of the aligned Cs^+ ion pair, r_i (Figure 8a) shows a ~7.0% increase from

2.933(8) to 3.138(19) Å due to thermal expansion of the lattice. However, this is then followed by a sharp increase of ~6.3% to 3.337(17) Å in the 30 K range of the transformation plateau between 266 and 296 K (Figure S8). Such a jump likely signifies a decrease in the interaction between the O_2^- units and the aligned Cs^+ ion pair. While the O_2^- unit in the tetragonal structure maintains its alignment, and therefore its tilt away from the crystallographic axis (Figure S7), a translation to a more symmetric location within the surrounding Cs^+ polyhedron (Figure 8a) could be the signature of orbital order melting in the tetragonal phase. The temperature-dependent features of the sudden translational shift is most clearly observed in the evolution of the change in the O_2^- position relative to the center of mass of the Cs^+ polyhedron, $R_{(O_2^-)}$–$R_{(O_2^-)2K}$ with increasing temperature (Figure 8b). The shift of the O_2^- unit causes an increased steric interaction with the Cs^+ ions that reside above and below the bonding axis of the O_2^- anion, resulting in an expansion in the direction that the molecules are approximately aligned with, namely, the crystallographic *c* axis.

The transformation plateau can therefore be explained by one of two possible scenarios, brought about by these subtle structural changes:

(1) The changes in the polyhedral environment surrounding the O_2^- unit upon warming above 266 K lead to increased steric hindrance for molecular rotation. There is no longer sufficient thermal energy to overcome the increased energy barrier ($k_B T < E_a$) and so the rotation required for the tetragonal to cubic, charge-order-melting, conversion is hindered. This creates a plateau in the temperature dependence of the phase fractions until the material is heated to a temperature where the thermal energy is large enough to overcome this barrier ($k_B T > E_a$), i.e., above 296 K.

(2) The tetragonal-to-cubic transformation is accompanied by the melting of charge order.[14] At 266 K, where the molecule moves away from its *aligned* pair of Cs^+ ions, and presumably orbital order melts, electronic overlap is reduced. Such a reduction would lead to an increased barrier to the charge hopping necessary to allow delocalization and charge-order melting. As in the previous scenario, upon heating above 296 K, thermal energy is enough to overcome this energy barrier ($k_B T > E_a$), allowing charge order to melt and conversion from the tetragonal to cubic phase to proceed to completion.

The current data are not able to distinguish between these two scenarios, while previously published reports on this material have not identified this region of halted transformation. Inhomogeneities in the grain size distribution arising from the martensitic nature of the transition (vide infra) may also be contributing to the emergence of the transformation plateau and the reentrant kinetic arrest of the T phase.

The sluggish and highly hysteretic behavior of the transformation, due to molecular rotations, follows a thermally activated behavior.[14] When the sample is cooled rapidly via “deep quenching” through the temperature region where molecular rotation is possible (195 K > *T* > 147 K), long-range charge order is not observed and the valence disordered, cubic $(Cs^+)_4(O_2^{4/3-})_3$ structure is found as the kinetic product. On the other hand, when the sample is cooled “ultraslowly”, transformation to the thermodynamic charge-ordered,

tetragonal $(Cs^+)_4(O_2^-)_2(O_2^{2-})$ product is achieved. However, despite cooling at a rate of 1.68 K h^{-1}, conversion of only 76.51(7)% is achieved, suggesting the presence of a significant energy barrier. Upon heating from the base temperature following both "ultraslow-cooling" and "deep-quenching" protocols, the same phase fraction developments are observed, with the onset of the cubic-to-tetragonal structural transformation found at ~160 K, setting a value for the magnitude of the activation barrier for the C → T phase change. Upon further heating, the phase change is reversed above 195 K when the tetragonal phase begins to transform back to the cubic one. A further change in behavior occurs in the range 266 K < T < 296 K, when the to-cubic transformation is enhanced, presumably because of either steric hindrance or a reduction in the electronic overlap necessary for the melting of charge order (vide supra), and so any tetragonal fraction remaining is frozen until the sample is heated above 296 K, setting a value for the magnitude of the activation barrier for the T → C phase change in this temperature range. Figure 9 shows a schematic representation of the temperature evolution of the free energy of the system and the barrier to transformation inferred from these behaviors together with a summary of the phase assemblage in the temperature range covered by the present experiments for the various thermal protocols.

While the extreme air and moisture sensitivity of Cs_4O_6 has so far complicated measurements of the thermodynamic data, the observation of hysteresis, volume step change, and phase coexistence provides the signature of a first-order phase transition driven by molecular rotation of the dioxygen units and the accompanying charge ordering. These traits are also observed in the wide range of martensitic materials. In order to be able to classify a phase transition as martensitic, several criteria must be met: the phase change must be a shear-dominant, lattice-distortive, diffusionless transformation occurring by nucleation and growth.[15] In the case of Cs_4O_6, the structural change during the transition is not a reconstructive process but a diffusionless one. This is clear when considering Figure 7a,b because the underlying arrangement of the Cs^+ network and the dioxygen units remains unchanged but molecular rotation of the O_2^- units occurs, implying the absence of long-range diffusional motion of the ions during the transition. The significant, ~1.0%, lattice contraction as a result of the transition confims fulfillment of the lattice-distortive criterion, while the symmetry change from cubic to tetragonal is consistent with a shear-dominant mechanism rather than a purely dilatational transformation. The nucleation and growth descriptor, separating martensitic from quasi-martensitic transformation classifications, is the most difficult to confirm with respect to the currently available data. The large hysteresis and phase coexistence are suggestive of a nucleation and strain-driven mechanism. In martensitic systems, the microstructure, grain size, and crystal defects are known to play important roles in the observed transition behavior because of the requirement of the growth to proceed through domain boundary motion.[27,28] The results described in ref 14 are obtained from samples synthesized by thermal decomposition of CsO_2,[29] while the results presented here and in other earlier reports are from samples prepared by the solid-state reaction of CsO_2 and Cs_2O.[8,12] The hysteresis widths for the samples prepared by solid-state reaction and by thermal decomposition are 120 and 50 K, respectively, suggesting the existence of different microstructures and defect concentrations, as expected when different preparative methods affect the transformation kinetics and thermodynamics. Therefore, the

overall phenomenology of the phase change in Cs_4O_6 appears to confirm its classification as a martensitic transformation.

CONCLUSION

In conclusion, we have presented NPD structural measurements on the molecular sesquioxide Cs_4O_6 as a function of the temperature following a variety of thermal protocols. We have confirmed that at low temperatures the ground-state structure of Cs_4O_6 is tetragonal and incorporates two symmetry-inequivalent dioxygen units in the ratio 1:2 and with bond lengths at 10 K of 1.528(6) and 1.345(4) Å, characteristic of diamagnetic peroxide and paramagnetic ($S = ½$) superoxide anions, respectively, clear evidence of charge and orbital order. Notably, however, the emergence of static order and the transition to magnetic long-range order are suppressed because of geometric frustration: the superoxide anions are arranged on a distorted pyrochlore lattice of vertex-sharing tetrahedra, resulting in a highly frustrated 3D spin topology, precluding the transition to a magnetically ordered state.

The cubic → (contracted) tetragonal structural transition is incomplete, with a sizable fraction of the cubic phase (~25%) surviving to low temperatures even when the sample is cooled extremely slowly at a rate of 1.68 K h^{-1} over a period of ~7 days. In fact, the cubic phase can be kinetically arrested down to 1.8 K when it is subjected to “deep-quenching” thermal protocols; only a single type of dioxygen unit is present in this phase. This kinetic arrest of the transformation implies nonequilibrium behavior. An anomalously short bond distance is found from diffraction for this dioxygen unit but after correction for the large librational motion; the “true” value falls in the range 1.308(2)–1.457(3) Å, consistent with valency delocalization, leading to an average dioxygen charge between that of superoxide and peroxide anions. Monitoring the composition of the tetragonal/cubic phase assemblage upon heating between 1.8 and 320 K reveals a series of successive interconversions, indicative of the comparable magnitude of the transformation barriers to the thermal energies; the cubic component begins to transform to tetragonal at ~164 K but the trend is reversed above 195 K, when the tetragonal phase begins to revert back to cubic. This is followed by a plateau between 266 and 296 K when the relative phase fractions remain invariant, following which the tetragonal phase fully converts to cubic, with charge and orbital order completely melting upon further heating. The hysteretic nature of the transition is evident from the structural results obtained upon cooling when the onset of conversion to the tetragonal phase is found at 198 K (hysteresis width at ~120 K). Arresting of the transformation upon cooling occurs at 147 K. The diffusionless character of the cubic → tetragonal transformation, where, besides rotation of the molecular dioxygen units, the same relative structural motif is maintained through the symmetry lowering and anisotropic lattice strain, classifies this as a martensitic transformation.

Supplementary Material

Refer to Web version on PubMed Central for supplementary material.

ACKNOWLEDGMENTS

We thank ISIS (GEM data DOI10.5286/ISIS.E.24091149) for access to neutron facilities. This work was financially supported by Grants-in-Aid for Scientific Research (JSPS KAKENHI Grants JP17H05139, JP18H04303, JP18K18724, and JP19H04590) by the Ministry of Education, Culture, Sports, Science and Technology, Japan, by the Czech OP VVV project MATFUN (Grant CZ.02.1.01/0.0/0.0/15_003/0000487), and by the European Union/JST FP7-NMP-2011-EU-Japan project LEMSUPER (Contract NMP3-SL-2011-283214).

REFERENCES

(1). Zadik RH; Takabayashi Y; Klupp G; Colman RH; Ganin AY; Potocnik A; Jeglic P; Arcon D; Matus P; Kamaras K; et al. Optimized Unconventional Superconductivity in a Molecular Jahn-Teller Metal. Sci. Adv 2015, 1, No. e1500059. [PubMed: 26601168]

(2). Takabayashi Y; Menelaou M; Tamura H; Takemori N; Koretsune T; Štefančič A; Klupp G; Buurma AJC; Nomura Y; Arita R; et al. π-Electron S = 1/2 Quantum Spin-Liquid State in an Ionic Polyaromatic Hydrocarbon. Nat. Chem 2017, 9, 635. [PubMed: 28644474]

(3). Jansen M; Korber N Neue Untersuchungen zu Preparation und Struktur von Rb_4O_6. Z. Anorg. Allg. Chem 1991, 598, 163.

(4). Jansen M; Hagenmayer R; Korber N Rb_4O_6 Studied by Elastic and Inelastic Neutron Scattering. C. R. Acad. Sci., Ser. IIc: Chim 1999, 2, 591.

(5). Robin MB; Day P Mixed Valence Chemistry - A Survey and Classification. Adv. Inorg. Chem. Radiochem 1968, 10, 247.

(6). Mixed Valency Systems: Applications in Chemistry, Physics and Biology; Prassides K, Ed.; Springer: Dordrecht, The Netherlands, 1991.

(7). Helms A; Klemm W Über die Kristallstrukturen der Rubidium- und Cäsiumsesquioxyde. Z. Anorg. Allg. Chem 1939, 242, 201.

(8). Winterlik J; Fecher G; Jenkins C; Medvedev S; Felser C; Kübler J; Mühle C; Doll K; Jansen M; Palasyuk T; et al. Exotic Magnetism in the Alkali Sesquioxides Rb_4O_6 and Cs_4O_6. Phys. Rev. B: Condens. Matter Mater. Phys 2009, 79, 214410.

(9). Attema JJ; de Wijs GA; Blake GR; de Groot RA Anionogenic Ferromagnets. J. Am. Chem. Soc 2005, 127, 16325. [PubMed: 16287327]

(10). Winterlik J; Fecher GH; Felser C; Mühle C; Jansen M Challenging the Prediction of Anionogenic Ferromagnetism for Rb_4O_6. J. Am. Chem. Soc 2007, 129, 6990. [PubMed: 17500525]

(11). Winterlik J; Fecher GH; Jenkins CA; Felser C; Mühle C; Doll K; Jansen M; Sandratskii LM; Kübler J Challenge of Magnetism in Strongly Correlated Open-Shell 2p Systems. Phys. Rev. Lett 2009, 102, 016401. [PubMed: 19257217]

(12). Arčon D; Anderle K; Klanjšek M; Sans A; Mühle C; Adler P; Schnelle W; Jansen M; Felser C Influence of O2Molecular Orientation on p-Orbital Ordering and Exchange Pathways in Cs_4O_6. Phys. Rev. B: Condens. Matter Mater. Phys 2013, 88, 224409.

(13). Sans A; Nuss J; Fecher GH; Mühle C; Felser C; Jansen M Structural Implications of Spin, Charge, and Orbital Ordering in Rubidium Sesquioxide, Rb_4O_6. Z. Anorg. Allg. Chem 2014, 640, 1239.

(14). Adler P; Jeglič P; Reehuis M; Geiß M; Merz P; Knaflič T; Komelj M; Hoser A; Sans A; Janek J; et al. Verwey-Type Charge Ordering Transition in an Open-Shell *p*-Electron Compound. Sci. Adv 2018, 4, No. eaap7581. [PubMed: 29372183]

(15). Christian J; Olson G; Cohen M Classification of Displacive Transformations : What is a Martensitic Transformation? J. Phys. IV 1995, 5, C8-3–C8-10.

(16). Larson AC; von Dreele R General Structure Analysis System (GSAS). Los Alamos Natl. Lab. Rep. LAUR 2004, 86–748.

(17). Helms A; Klemm W Über die Kristallstrukturen der Rubidium- und Cäsiumsesquioxyde. Z. Anorg. Allg. Chem 1939, 242, 201.

(18). Dudarev VY; Tsentsiper AB; Dobrolyubova MS Phase-Transitions in Epiperoxides of Rubidium and Cesium. Kristallografiya 1973, 18, 759.

(19). Momma K; Izumi F *VESTA 3* for Three-Dimensional Visualization of Crystal, Volumetric and Morphology Data. J. Appl. Crystallogr 2011, 44, 1272.

(20). Bremm T; Jansen M Verfeinerung der Kristallstruktur von K_2O_2. Z. Z. Anorg. Allg. Chem 1992, 610, 64.

(21). Seyeda H; Jansen M A Novel Access to Ionic Superoxides and the First Accurate Determination of the Bond Distance in O_2^-. J. Chem. Soc., Dalton Trans 1998, 875, 875.

(22). Shahee A; Kumar D; Shekhar C; Lalla NP Kinetic Arrest of the First-Order R-3c to Pbnm Phase Transition in Supercooled $La_xMnO_{3+\delta}$ (x = 1 and 0.9). J. Phys.: Condens. Matter 2012, 24, 225405. [PubMed: 22592293]

(23). Banerjee A; Mukherjee K; Kumar K; Chaddah P Ferromagnetic Ground State of the Robust Charge-Ordered Manganite $Pr_{0.5}Ca_{0.5}MnO_3$ Obtained by Minimal Al Substitution. Phys. Rev. B: Condens. Matter Mater. Phys 2006, 74, 224445.

(24). Chaddah P; Kumar K; Banerjee A Devitrification and Recrystallization of Magnetic Glass $La_{0.5}Ca_{0.5}MnO_3$. Phys. Rev. B: Condens. Matter Mater. Phys 2008, 77, 100402.

(25). Trump BA; Koohpayeh SM; Livi KJT; Wen JJ; Arpino KE; Ramasse QM; Brydson R; Feygenson M; Takeda H; Takigawa M; Kimura K; Nakatsuji S; Broholm CL; McQueen TM Universal Geometric Frustration in Pyrochlores. Nat. Commun 2018, 9, 2619. [PubMed: 29976983]

(26). Sibille R; Lhotel E; Ciomaga Hatnean M; Nilsen GJ; Ehlers G; Cervellino A; Ressouche E; Frontzek M; Zaharko O; Pomjakushin V; et al. Coulomb Spin Liquid in Anion-Disordered Pyrochlore $Tb_2Hf_2O_7$. Nat. Commun 2017, 8, 892. [PubMed: 29026077]

(27). Cugini F; Porcari G; Rimoldi T; Orsi D; Fabbrici S; Albertini F; Solzi M On the Broadening of the Martensitic Transition in Heusler Alloys: From Microscopic Features to Magnetocaloric Properties. JOM 2017, 69, 1422.

(28). Dunand DC; Müllner P Size Effects on Magnetic Actuation in Ni-Mn-Ga Shape-Memory Alloys. Adv. Mater 2011, 23, 216. [PubMed: 20957766]

(29). Merz P; Schmidt M; Felser C; Jansen M Thermo-Analytical Investigations on the Superoxides AO_2 (*A* = K, Rb, Cs), Revealing Facile Access to Sesquioxides A_4O_6. Z. Anorg. Allg. Chem 2017, 643, 544.

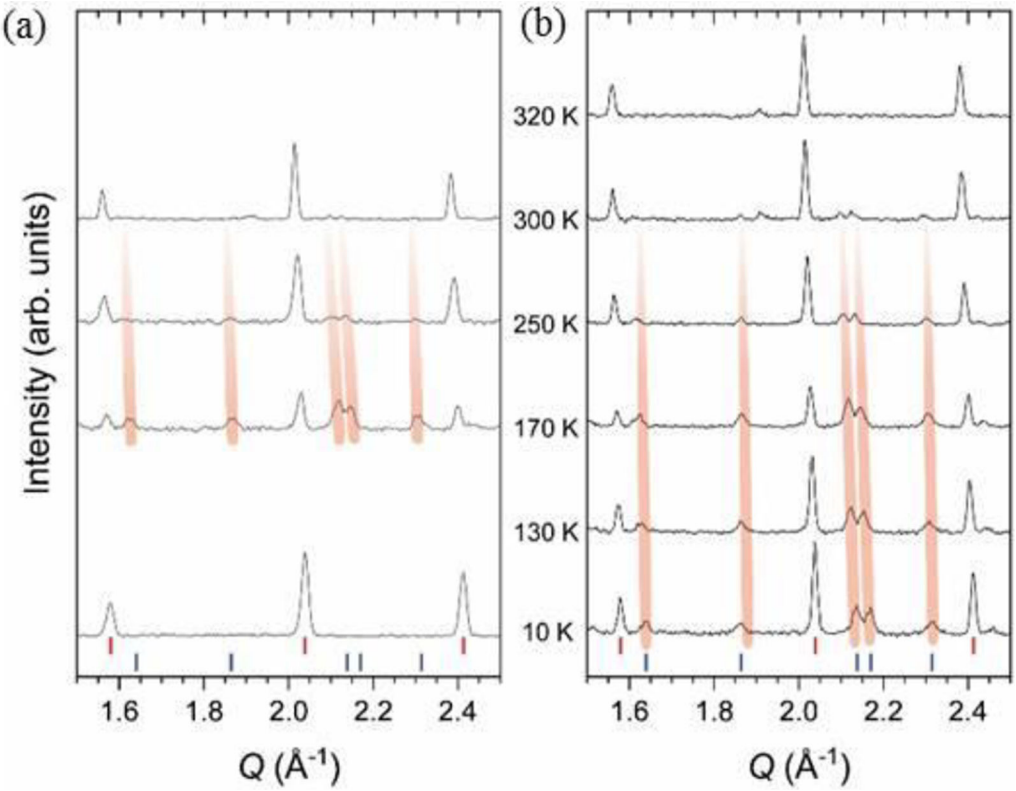

Figure 1.

Selected regions of the NPD data collected with the BT1 diffractometer upon heating from 10 K after different cooling protocols: (a) “deep-quenching” procedure; (b) “slow-cooling” procedure. Tick marks represent reflection positions for the cubic (top red set) and tetragonal (bottom blue set) cells. Profiles are offset for clarity, and the evolution of the tetragonal reflections with temperature is highlighted.

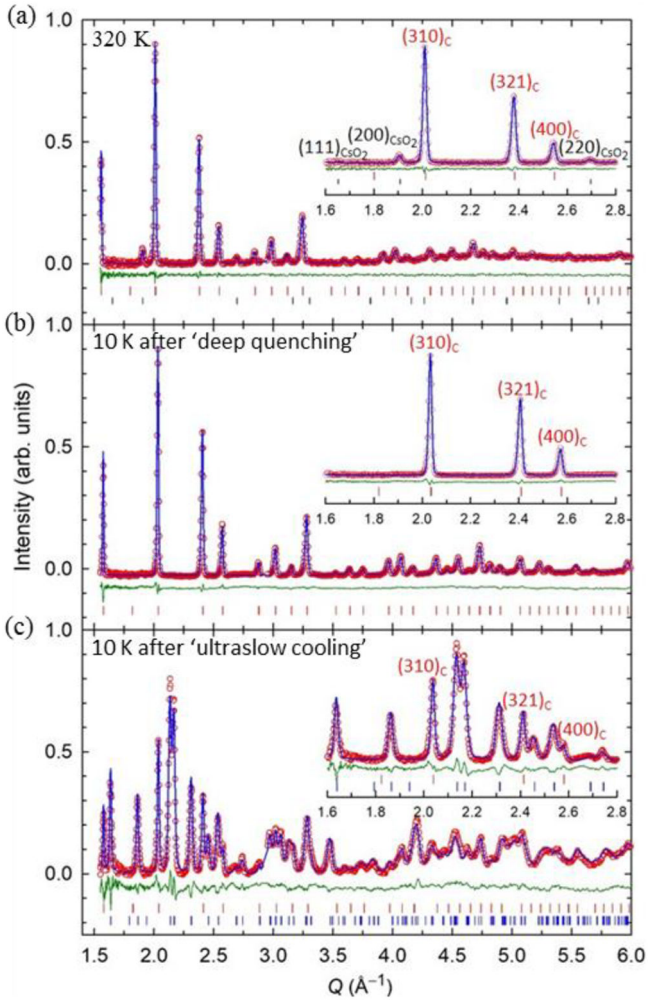

Figure 2.

Observed (red circles), calculated (blue lines), and difference (green lines) plots of the final Rietveld refinements of the tof-NPD data (detector bank 4) of Cs_4O_6 at 320 K (a), at 10 K after "deep quenching" (b), and at 10 K after "ultraslow cooling" (c). The red, blue, and black ticks in each panel mark the reflection positions of the cubic Cs_4O_6, tetragonal Cs_4O_6, and impurity cubic CsO_2 phases, respectively. The contribution from the vanadium sample holder in the range $Q = 2.85–2.95$ Å^{-1} is excluded from the refinements. The inset in each panel displays an expanded view ($Q = 1.6–2.8$ Å^{-1}) of the respective diffraction profile, with the observed reflections of the cubic Cs_4O_6 and impurity cubic CsO_2 phases labeled by their (*hkl*) Miller indices in red and black, respectively. The unlabeled reflections in the inset of the lower panel arise from tetragonal Cs_4O_6.

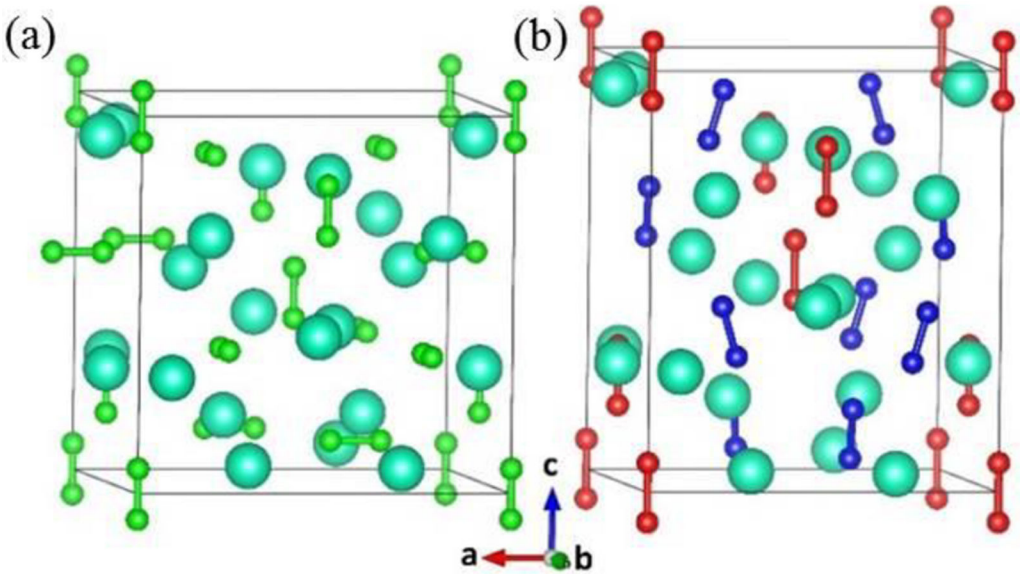

Figure 3.

(a) Cubic (C) and (b) tetragonal (T) (right) crystal structures of mixed-valent Cs_4O_6. The molecular formula of the compound can be depicted as $(Cs^+)_4(O_2^{4/3-})_3$ and $(Cs^+)_4(O_2^{2-})(O_2^-)_2$, respectively. The cubic (space group $I\bar{4}3d$) unit cell is displayed with an origin shift of $(-\frac{1}{2}, -1, -\frac{1}{8})$ for ease of comparison with that of the tetragonal (space group $I\bar{4}2d$) structure. Green, red, and blue dimers represent valency-delocalized $(O{-}O)^{4/3-}$, peroxide $(O{-}O)^{2-}$, and superoxide $(O{-}O)^-$ anions, respectively. Cs^+ cations are shown as larger turquoise spheres. Prepared using *VESTA3*.[19]

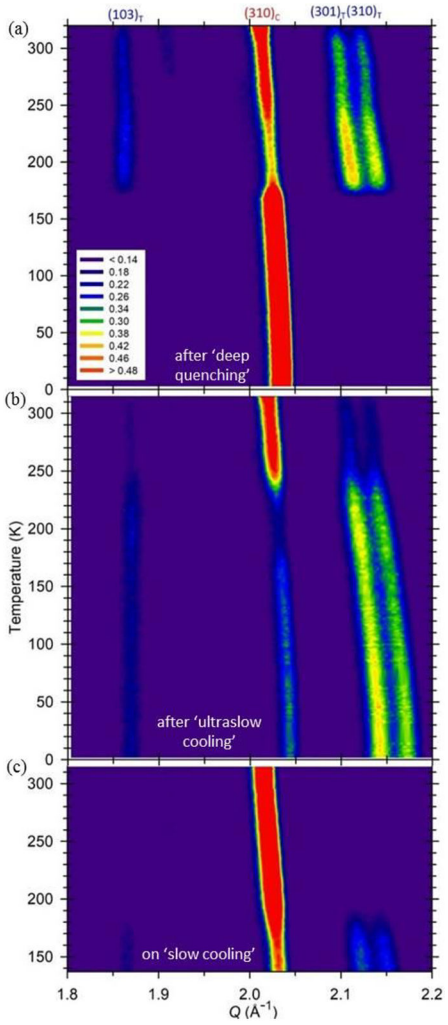

Figure 4.

Temperature response of the diffraction patterns of Cs_4O_6 (detector bank 4) in the vicinity of the cubic (310) Bragg reflection (a) upon warming from 1.8 to 320 K after “deep quenching”, (b) upon warming from 1.8 to 320 K after “ultraslow cooling”, and (c) upon “slow cooling” from 320 to 140 K (lower panel). Observed peaks are labeled with their corresponding Miller indices.

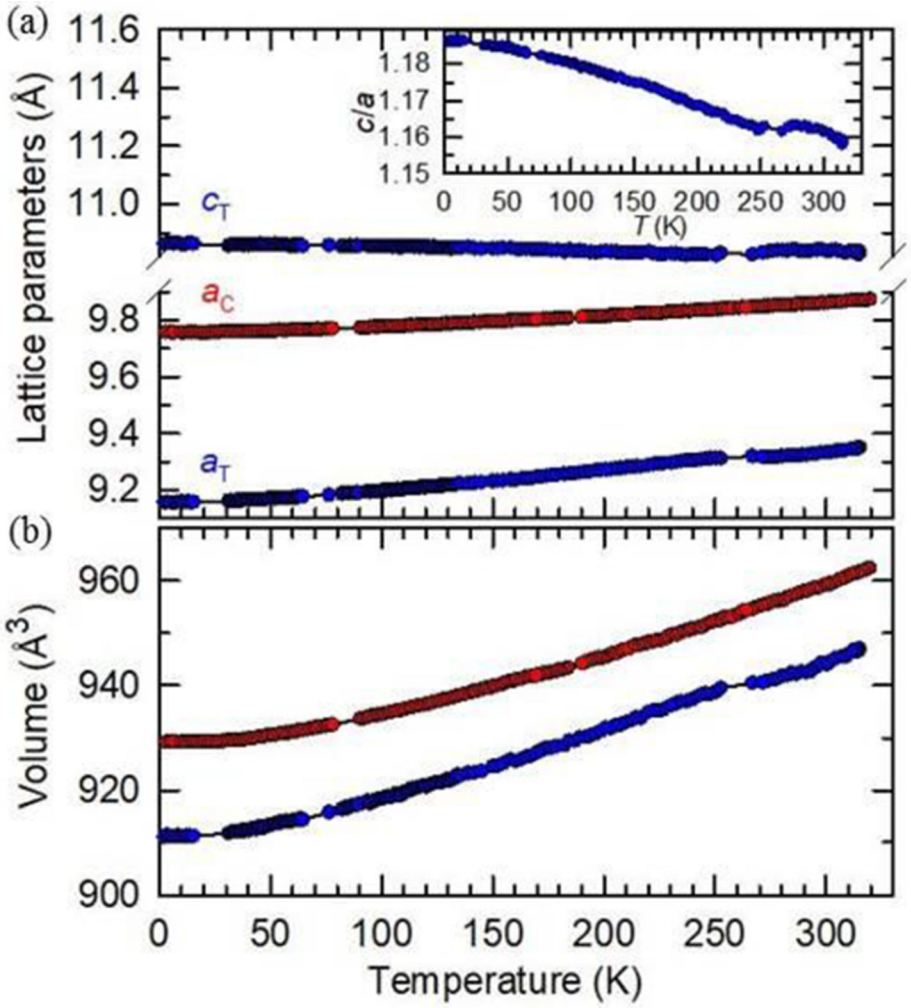

Figure 5.

Temperature evolution of the lattice constants (a) and the unit cell volume (b) of cubic (red circles) and tetragonal (blue circles) Cs_4O_6 extracted from tof-NPD data collected upon warming from 1.8 to 320 K after “deep-quenching” and “ultraslow-cooling” procedures, respectively. The inset in the top panel shows the temperature dependence of the *c*/*a* ratio in the tetragonal phase. Gaps between data points are due to neutron beam interruptions in the course of data acquisition. Solid lines are guides to the eye.

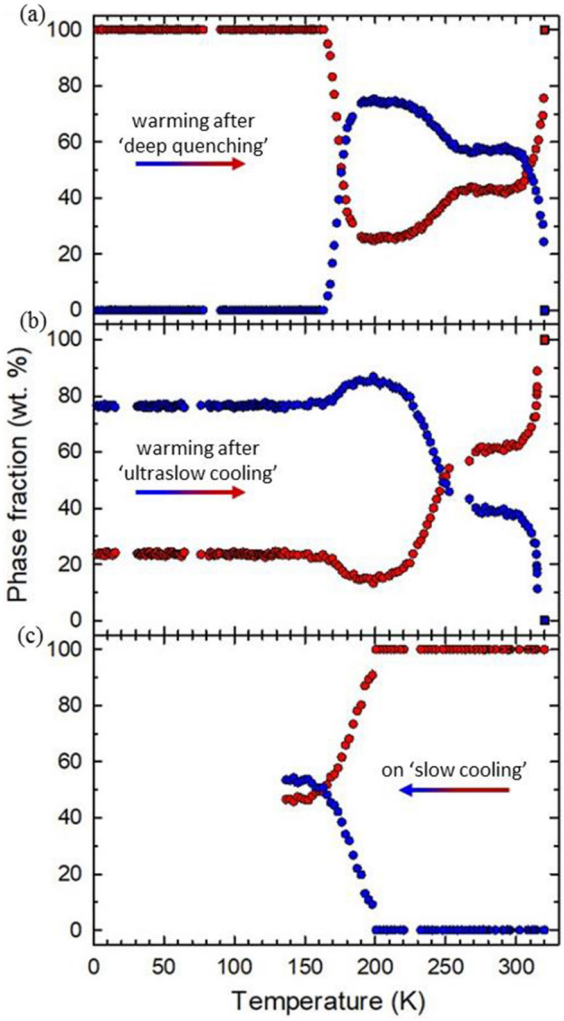

Figure 6.

Temperature evolution of the phase fractions of cubic (red circles) and tetragonal (blue circles) Cs_4O_6 (a) upon warming from 1.8 to 320 K after "deep quenching", (b) upon warming from 1.8 to 320 K after "ultraslow cooling", and (c) upon "slow cooling" from 320 to 140 K. Squares represent data obtained at 320 K after thermal equilibration of the sample for 2 h. Arrows in each panel indicate the direction of tof-NPD data collection.

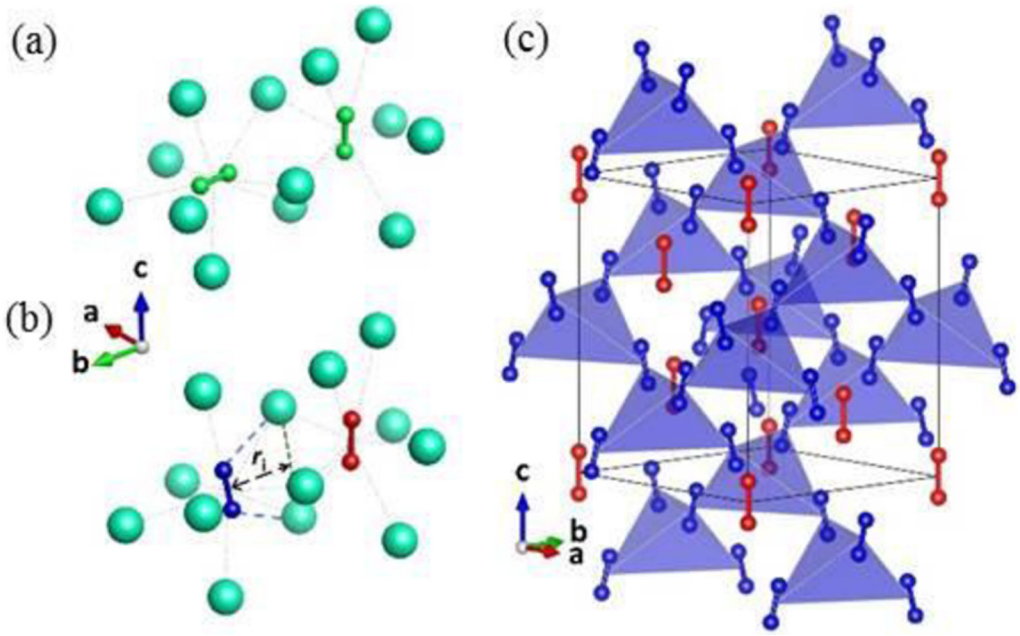

Figure 7.

Local structural environment of (a) $O_2^{4/3-}$ molecules (green spheres) and Cs^+ ions (turquoise spheres) in the cubic structure and (b) charge-ordered O_2^- (blue spheres) and O_2^{2-} (red spheres) in the tetragonal structure. The dashed lines show the Cs^+ ions with near-parallel alignment to the O_2^- molecular axis, and r_i labels the distance between the center of the O_2^- anion and the midpoint of the separation of the pair of Cs^+ ions with which it is aligned, as discussed in the text. (c) Shaded tetrahedra defining the distorted pyrochlore arrangement of the magnetically active O_2^- units in the tetragonal structure (the Cs^+ ions are omitted for clarity).

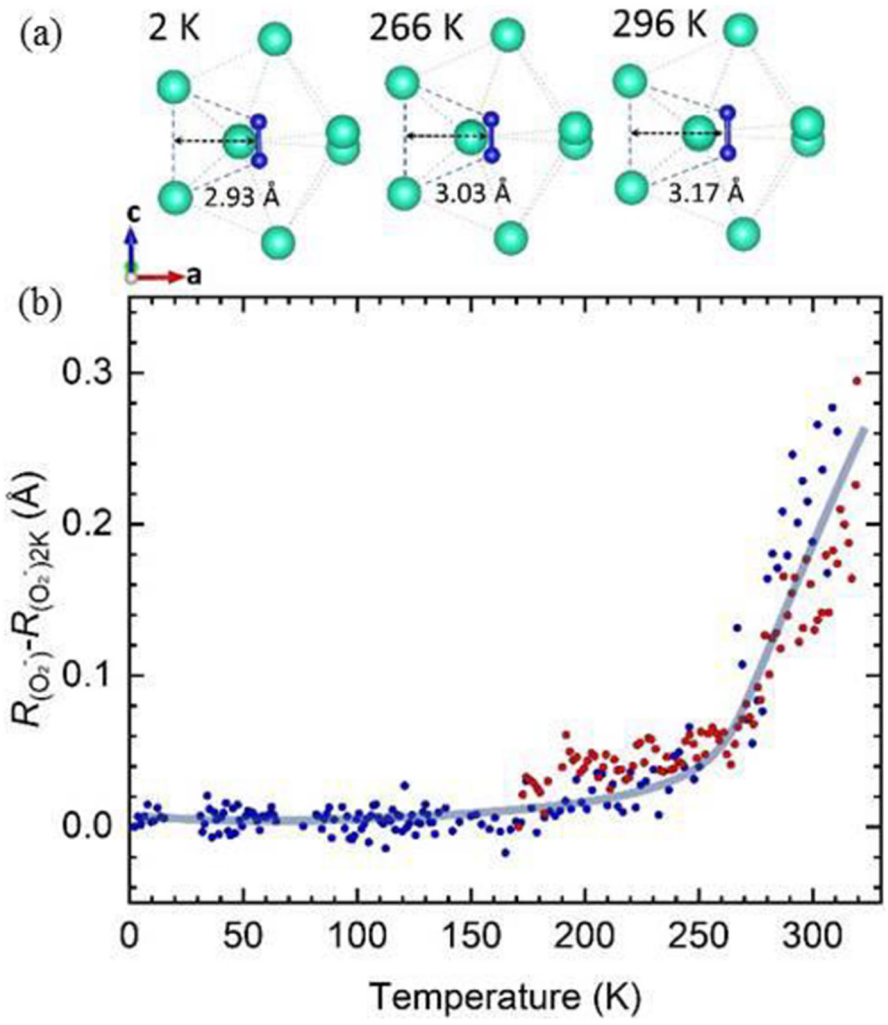

Figure 8.

(a) Schematic representation of the change in the O_2^- (blue spheres) local environment with increasing temperature highlighting the translational shift of the molecule within the surrounding Cs^+ (turquoise spheres) polyhedron. The thick dashed lines identify the Cs^+ pair, which is approximately aligned with the O_2^- bonding axis. (b) Temperature evolution of the position of the O_2^- unit within the surrounding Cs^+ polyhedron, $R_{(O_2^-)}$ relative to that at 2 K, $R_{(O_2^-)2K}$. Blue and red circles are from refined data after ultraslow cooling and deep quenching, respectively. The line through the points is a guide to the eye.

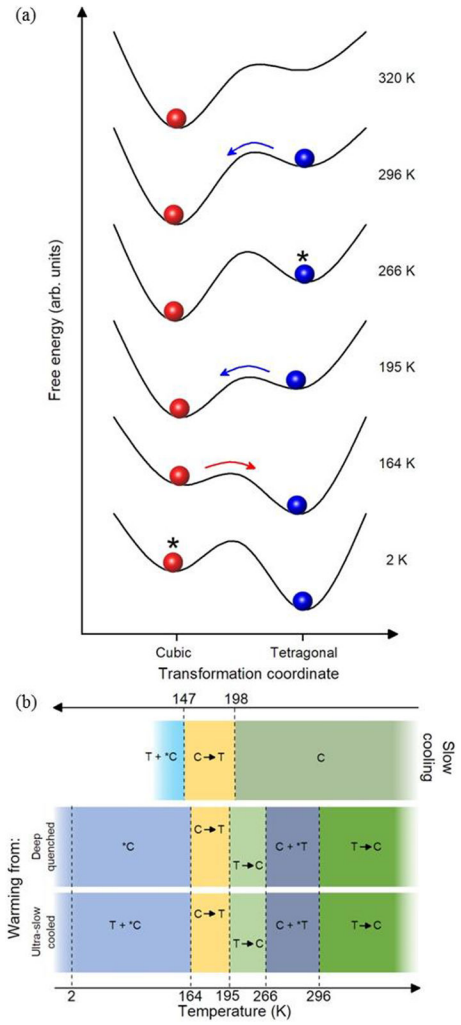

Figure 9.

(a) Schematic representation of the evolution of the free energies of the cubic (red) and tetragonal (blue) phases with temperature. Directional arrows show the temperatures where $E_a < k_B T$ so conversion is both allowed and spontaneous. Asterisks mark states that are thermodynamically unstable but trapped by kinetic arrest. (b) Observed phases (C = cubic; T = tetragonal) and transformation behavior during the measured thermal protocols. Asterisks have the same meaning as that in part a.

Table 1.

Refined Structural and Goodness-of-Fit Parameters from Rietveld Refinement Fits of the tof-NPD Data of Cs_4O_6 Collected on a GEM Diffractometer at Selected Temperatures[a]

	temperature		
	320 K	**10 K**	**10 K**
cooling protocol	heated from ambient *T*	deep quenching	ultraslow cooling
Cs_4O_6 phase composition	cubic only[b]	cubic only	cubic, 23.5(2)%; tetragonal, 76.51(7)%
		Cubic Structure	
space group	$I\bar{4}3d$	$I\bar{4}3d$	$I\bar{4}3d$
a_C (Å)	9.86744(8)	9.75760(5)	9.7381(2)
V_C (Å^3)	960.76(2)	929.03(2)	923.48(5)
Cs *x/a = y/b = z/c*	0.9464(1)	0.94638(6)	0.9460(2)
Cs U_{iso} (Å^2)	0.0560(8)	0.0207(3)	0.024(1)
Cs occupancy	1	1	1
O *x/a, y/b, z/c*	0.5606(2), 0, 0.75	0.5580(1), 0, 0.75	0.55790(5), 0, 0.75
O U_{11}, U_{22}, U_{33} (Å^2)	0.062(2), 0.121(2), 0.044(1)	0.0341(7), 0.0659(8), 0.0094(5)	0.026(2), 0.086(3), 0.023(3)
O U_{12}, U_{13}, U_{23} (Å^2)	0, 0, 0.009(1)	0, 0, 0.0045(5)	0, 0, 0.003(2)
O occupancy	1	1	1
O—O (Å)	1.272(3)	1.308(2)	1.307(1)[c]
		Tetragonal Structure	
space group			$I\bar{4}2d$
$a_T = b_T$, c_T (Å)			9.1586(2), 10.8653(5)
V_T (Å^3)			911.38(5)
Cs *x/a, y/b, z/c*			0.3034(2), 0.0555(2), 0.0474(2)
Cs U_{iso} (Å^2)			0.0071(4)
Cs occupancy			1
O(1) *x/a, y/b, z/c*			0, 0, 0.0703(3)
O(1) U_{11}, U_{22}, U_{33} (Å^2)			0.011(1), 0.005(2), 0.015(2)
O(1) U_{12}, U_{13}, U_{23} (Å^2)			0.012(1), 0, 0
O(1) occupancy			1
O(2) *x/a, y/b, z/c*			0.3776(3), 0.7705(2), 0.1844(2)
O(2) U_{11}, U_{22}, U_{33} (Å^2)			0.045(2), 0.011(2), 0.017(1)
O(2) U_{12}, U_{13}, U_{23} (Å^2)			0.005(1), −0.006(1), 0.006(1)
O(2) occupancy			1
O(1)—O(1) (Å)			1.528(6)
O(2)—O(2) (Å)			1.345(4)
R_{wp} (%)	2.17	2.86	3.00
R_{exp} (%)	2.71	2.08	2.29

[a]The “deep-quenching” and “ultraslow-cooling” protocols used are described in the text. Estimated errors in the last digits are given in parentheses and indicate 1 standard deviation.

[b]The fraction of the coexisting impurity cubic CsO_2 phase ($a_{320\ K}$ = 6.5864(7) Å; space group $Fm\bar{3}m$) at 320 K refines to 4.9(2)% (Figure 2, top).

[c]Because of the small fraction of the cubic phase under these conditions, the Rietveld refinement was performed after the introduction of an O—O bond distance restraint at 1.310 Å with a 0.005 tolerance and a restraint weight of 40.